Static load-carrying behavior and material properties of additively manufactured gears (PBF-LB/M, 16MnCr5)

Markus Brummer
Department of Mechanical Engineering, School of Engineering and Design, Gear Research Center (FZG), Technical University of Munich, Munich, Germany
Karl Jakob Raddatz
McKinsey & Company, Inc. (former member of FZG), Munich, Germany
Matthias Moritz Schmitt and Georg Schlick
Fraunhofer-Institute for Casting, Composite and Processing Technology (IGCV), Augsburg, Germany
Thomas Tobie
Department of Mechanical Engineering, School of Engineering and Design, Gear Research Center (FZG), Technical University of Munich, Munich, Germany
Rüdiger Daub
Fraunhofer-Institute for Casting, Composite and Processing Technology (IGCV), Augsburg, Germany and Department of Mechanical Engineering, School of Engineering and Design, Institute for Machine Tools and Industrial Management (iwb), Technical University of Munich, Munich, Germany, and
Karsten Stahl
Department of Mechanical Engineering, School of Engineering and Design, Gear Research Center (FZG), Technical University of Munich, Munich, Germany

Abstract

Purpose – Numerous metals can be processed using the additive manufacturing process laser-based powder bed fusion of metals (PBF-LB/M, ISO/ASTM 52900). The main advantages of additive manufacturing technologies are the high degree of design freedom and the cost-effective implementation of lightweight structures. This could be profitable for gears with increased power density, combining reduced mass with considerable material strength. Current research on additively manufactured gears is focused on developing lightweight structures but is seldom accompanied by simulations and even less by mechanical testing. There has been very little research into the mechanical and material properties of additively manufactured gears. The purpose of this study is to investigate the behavior of lightweight structures in additively manufactured gears under static loads.

Design/methodology/approach – This research identifies the static load-carrying capacity of helical gears with different lightweight structures produced by PBF-LB/M with the case hardening steel 16MnCr5. A static gear loading test rig with a maximum torque at the pinion of $T_1 = 1200$ Nm is used. Further focus is set on analyzing material properties such as the relative density, microstructure, hardness depth profile and chemical composition.

Findings – All additively manufactured gear variants show no failure or plastic deformation at the maximum test load. The shaft hub connection, the lightweight hub designs and the gearing itself are stable and intact regarding their form and function. The identified material characteristics are comparable to conventionally manufactured gears (wrought and machined), but also some particularities were observed.

Originality/value – This research demonstrates the mechanical strength of lightweight structures in gears. Future research needs to consider the dynamic load-carrying capacity of additively manufactured gears.

Keywords Material properties, Additive manufacturing, Powder bed fusion, Lightweight, 16MnCr5, PBF-LB/M, Helical gear, Lightweight

Paper type Research paper

The current issue and full text archive of this journal is available on Emerald Insight at: **https://www.emerald.com/insight/1355-2546.htm**

Rapid Prototyping Journal
29/11 (2023) 117–130
Emerald Publishing Limited [ISSN 1355-2546]
[DOI 10.1108/RPJ-02-2023-0035]

© Markus Brummer, Karl Jakob Raddatz, Matthias Moritz Schmitt, Georg Schlick, Thomas Tobie, Rüdiger Daub and Karsten Stahl. Published by Emerald Publishing Limited. This article is published under the Creative Commons Attribution (CC BY 4.0) licence. Anyone may reproduce, distribute, translate and create derivative works of this article (for both commercial and non-commercial purposes), subject to full attribution to the original publication and authors. The full terms of this licence may be seen at http://creativecommons.org/licences/by/4.0/legalcode

Received 1 February 2023
Revised 27 June 2023
Accepted 27 August 2023

1. Introduction

Additive manufacturing has various advantageous properties in the production of components compared to conventional manufacturing processes. Upon the most frequently mentioned are design freedom, mass savings through lightweight structures and near-net shaping (Gebhardt, 2016; Gibson *et al.*, 2021; Milewski, 2017). The simple and cost-effective realization of lightweight structures plays an important role in the successful application of additive manufacturing (Kamps *et al.*, 2018). Lightweight designs are favored and gaining importance due to an increased pursuit of resource efficiency and elevated power densities. As a consequence of mass saving, the energy consumption in the application is reduced (Bartels *et al.*, 2020), which has positive effects on the environment and counteracts global warming.

Conventional manufacturing technologies, such as casting, turning, gear hobbing and grinding, limit the design freedom of lightweight structures due to manufacturability. In the case of gears, conventionally manufactured lightweight structures are usually implemented in the gear hub area between the shaft-hub connection and the gear rim (Niemann and Winter, 2003). A possible influence on the tooth root bending strength is considered by the rim thickness factor Y_B in ISO 6336–3 (2019). Negative aspects of lightweight structures can be unfavorable noise, vibration, harshness characteristics (Ramandani *et al.*, 2018) and an inappropriate design for the applied load. An increased material and mass saving are possible if the lightweight structure is optimally adapted to the load (Mura *et al.*, 2018).

Additive manufacturing opens up the possibility of load-customized structures and saving material specifically in areas with low stresses, e.g. by topology optimization (Gibson *et al.*, 2021; Milewski, 2017). Areas with low stresses can mainly be found in the region between the shaft-hub connection and the gear rim and also inside the tooth itself (Muminovic *et al.*, 2019). These areas can be used as design space for optimized lightweight structures. Several approaches have been developed to create and implement lightweight structures in gears by using additive manufacturing (Nguyen and Vignat, 2016; Mura *et al.*, 2018; Kamps *et al.*, 2018; Schmitt *et al.*, 2019). However, when following these approaches, the load-carrying capacity is seldom analyzed or even considered.

Nguyen and Vignat (2016) show an approach to generate periodical and non-periodical lightweight structures. A helical gear is used in the case study to demonstrate the approach. A mass saving of 50% by introducing the lightweight structure is stated, but the load the lightweight structure can withstand is not presented.

Kamps *et al.* (2017) combine TRIZ with biomimicry. With TRIZ, a problem is solved by abstracting the problem and finding suitable analogies in a database search. The main steps are the analysis of the part, abstract functional description, abstract biomimetic design, and final part design. The method is demonstrated for a gear and achieves a mass reduction of 28%.

Mura *et al.* (2018) focus their study on generating a spoke wheel in a six-step optimization procedure. The target parameters are to reduce mass, increase the first natural frequency (reduce noise) and keep or increase strength and stiffness, categorized by the static safety factor and the transmission error. Calculations for the static and fatigue strength are carried out between the different steps. The method is applied on a spur gear with bores, and a mass reduction of 2% is realized while the first natural frequency is increased by 180%.

Kamps *et al.* (2018) designed a lightweight structure with integrated cooling channels. Their approach uses Constructal Theory, a mathematical design approach, and, more specifically, point-to-circle flow with tree-shaped structures. Point-to-circle flow means "to distribute a fluid flow from a source S at a circle center to a number of points N lying on the circle with diameter d" (Kamps *et al.*, 2018). The material is then built around the fluid flows. Thus, the gear is designed from the inside out. The method is considered to maintain a first design concept, and further steps should be conducted to obtain an optimized material distribution.

Schmitt *et al.*, (2019) specify the design space between the shaft-hub connection and gear rim. The geometric limitations of the design space are based on the results of Brůžek and Leidich (2007), which recommend that the thickness above feather keys should not be below $1.8 \times m_n$ as well as ISO 6336-3 (2019) for gear rim thickness, based on a desired safety factor S_F and the rim thickness factor Y_B. The design space is then filled with bionically and topologically optimized structures considering the safety factor S_F and the maximum stress in the gear body. As a result, mass savings of 34% for the bionically optimized and 30% for the topologically optimized lightweight gears are achieved. The paper of Winkler *et al.* (2023) gives an overview of different lightweight designs and investigations into additively manufactured gears conducted in close cooperation with Schmitt *et al.* (2019). The presented experimental results will be further detailed in this and upcoming research paper.

Further examples of developed lightweight structures in gears but without describing a generally applicable approach can be found in Kulangara *et al.* (2018) (honeycomb structure), Ramandani *et al.* (2018) (cube and plane diagonal lattice), Concli and Della Torre (2021) (reticular structure) and Bulduk *et al.* (2022) (hexagonal lattice, spiral lattice and gyroid lattice).

Muminovic *et al.* (2019, 2020) investigate an approach to save mass within each gear tooth. The first research paper of Muminovic *et al.* (2019) addresses hollow gear teeth and finding a suitable shell thickness for an applied load by means of simulations. The suitable shell thickness is identified by evaluating the von Mises stress at different spots and considering the depth of Hertzian pressure. Lightweight teeth with von Mises stresses comparable to solid teeth are achieved with 2.5 mm shell thickness resulting in a mass reduction of 10%.

The second research paper of Muminovic *et al.* (2020) uses the same load for the simulations, but the shell thickness is reduced to 1.0 mm, and the hollow gear teeth are filled with different lightweight structures. Topological infills show lower stresses and fewer displacements compared to triangular infills. Topological infills taking up 60% of the hollow space show comparable von Mises stresses to a solid tooth, leading to a mass reduction of 16%.

In the above-mentioned research, only Ramandani *et al.* (2018), Schmitt *et al.* (2019), Concli and Della Torre (2021) and Bulduk *et al.* (2022) have successfully produced gears with lightweight structures using PBF-LB/M.

So far, only Bulduk *et al.* (2022) have conducted experimental investigations on the load-carrying capacity of lightweight structures of additively manufactured gears. The study focuses on the static load-carrying capacity. The gears

were produced by PBF-LB/M using the material AlSi10Mg with "standard production parameters" (Bulduk *et al.*, 2022) on an M 290 by EOS GmbH. The setup contained five additively manufactured gears, namely without lightweight structures (reference), hexagonal lattice, spiral lattice, gyroid lattice and material in the design space solidified with a different parameter set, leading to a porous structure. The spiral and hexagonal lattice failed at loads 42% and 3% below the load where the reference failed with tooth root breakage. The gyroid lattice did not fail, but tooth root breakage occurred at a 21% higher load than for the reference. The gear with two different parameter sets detached between the design space and gear rim at a load 42% lower than the reference.

The results of Bulduk *et al.* (2022) show that designing and producing gears with lightweight structures with comparable load-bearing capacities is a more highly sophisticated task than the current state of the art. In this investigation, helical gears with three different types of lightweight structures were manufactured by PBF-LB/M using the case hardening steel 16MnCr5. The gears were mechanically tested with a static load to identify the static load-carrying capacity of the lightweight structure. For the mechanical testing, a static gear loading test rig was used. Accompanying investigations included examinations to identify the microstructure, density, hardness depth profile, and chemical composition of the material, as well as measurements and ratings regarding the manufactured gear quality. The results were compared with the test results of conventionally manufactured gears.

2. Methods

2.1 Geometry of the test gears

For this investigation, helical gears with three different lightweight structures were manufactured. The tooth geometry is inspired by gears used in the automotive sector and is called type 1 (Table 1). Bionically and topologically optimized lightweight structures were developed by Schmitt *et al.* (2019) according to the design approach they developed. The lightweight designs were only realized on the wheels due to the available design space between the shaft-hub connection and gear rim (Table 2; Figure 1). The pinions were constructed without any lightweight structures due to the limited design space between the shaft-hub connection and gear rim.

2.2 Process chain for the production of the test gears

The gears were manufactured using PBF-LB/M according to the process chain for additively manufacturing gears defined by Schmitt *et al.* (2020a). PBF-LB/M is an additive manufacturing technology processing metal powder by laser beam fusion that creates a part by repeating three steps (Milewski, 2017):

1 applying a layer of powder with a recoater;
2 selective melting of the powder with a laser; and
3 lowering the building plate by the amount of the layer thickness.

Figure 2 shows a schematic setup of a PBF-LB/M machine.

The PBF-LB/M process was executed on an M 290 by EOS GmbH with a layer thickness $H = 30\ \mu m$ and an energy density $E_V = 86.5\ J/mm^3$ in an argon atmosphere while holding the building plate at a temperature $\vartheta_B = 80°C$. The used powder was 16MnCr5 (1.7131) according to DIN EN ISO 683–3 (2019) with spherical particles and a mean particle diameter $D_{50} = 42.4\ \mu m$. Considering the shrinkage during PBF-LB/M, an allowance of 0.2 mm was added on the hub and bore, and a protuberance of 0.1 mm on the tooth flanks.

After the building process was finished, stress relief heat treatment was carried out for 6 h at a temperature of 600°C in an argon atmosphere before electrical discharge machining the gears from the building plate and removing the support structures by machining. The case hardening steel was subsequently case-hardened (920°C carburization temperature; 840°C hardening temperature; 190°C tempering temperature) to achieve a case hardening depth $CHD_{550HV} = 0.8 + 0.2$ mm. The gears were mechanically cleaned by shot blasting and the plane surfaces, bore and tooth flanks were ground afterward.

2.3 Test equipment and test conditions

The static load-carrying capacity of the gears was tested on a static gear loading test rig (Figure 3), which was first used in the project LIGHTWEIGHTforging (Leonhardt *et al.*, 2020). The test rig applies a slowly increasing torque to the gear set. An electric motor drives a gear that meshes with a toothed rack to move it up and down with constant speed. The toothed rack is mounted on a lever arm that transfers the linear motion into a rotation on the gear shaft, transforming force into torque. The test pinion and measurement systems for the torque and rotation angles are mounted on the rotating gear shaft. The torque and rotation angle are measured with a 20 Hz sampling frequency. The test pinion meshes with the test wheel, which is mounted on a second gear shaft. The wheel shaft has high torsional stiffness and is fixed to close the flow of forces. The test rig configuration allows a repeatable installation of the

Table 1 Geometrical data of the type 1 test gear

Description	Symbol	Unit	Value	
			Pinion	Wheel
Number of teeth	z	–	25	27
Normal module	m_n	mm	3.3	
Helix angle	β	°	+18.0	−18.0
Face width	b	mm	14.0	16.0
Tip diameter	d_a	mm	94.00	101.00
Span over 4 teeth (nominal)	W_k	mm	36.206	35.673
Center distance	a	mm	91.5	

Source: By author

Table 2 Variants with lightweight structures on the wheels

Name	Description	Mass reduction
Type 1 noLB	Solid gear hubs, no lightweight structure realized	Reference
Type 1 LB-T	Topologically optimized lightweight structure	30.2%
Type 1 LB-B	Bionically optimized lightweight structure (biological model: bulrush)	24.5%
Type 1 LB-BO	Bionically optimized lightweight structure (biological model: bulrush) with further hub modifications (reduced thickness of lightweight structure and oval hub)	44.5%

Source: By author

Figure 1 CAD models of the different lightweight structures on the type 1 wheels

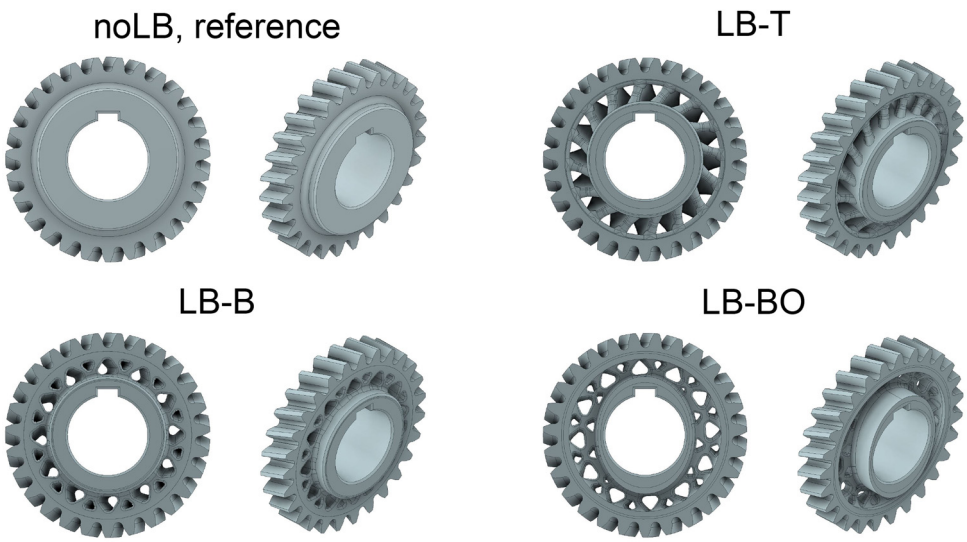

Source: By author

Figure 2 Schematic setup of a PBF-LB/M machine according to Winkler *et al.* (2023)

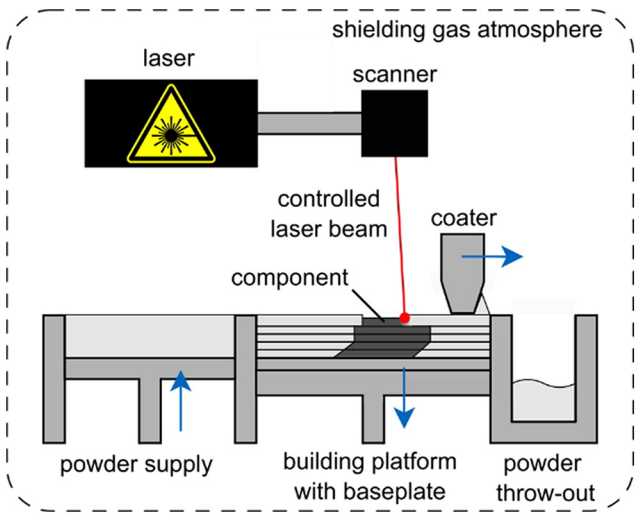

Source: Figure courtesy of Winkler *et al.* (2023)

mesh position. The maximum testing torque at the pinion shaft is $T_1 = 1200$ Nm and is limited by the dimensioning of the test rig. A test run consists of increasing the torque with a constant rate to $T_1 = 1200$ Nm and unloading the gear set when having reached the maximum torque or when plastic deformation occurs (nonlinearity in torque over time). The rate of torque increase is related to the torsional stiffness of the gear set. With high torsional stiffness, less angular rotation and time are needed to achieve the same torque as for low torsional stiffness, which requires more angular rotation and time.

Each wheel variant, depicted in Table 2, was paired with an additively manufactured pinion. A conventionally manufactured gear set (wrought and machined) with the same geometry and without lightweight structures was tested as a reference. The mesh position was determined in the single-pair tooth contact region to obtain maximum stresses on the gearing. The testing procedure was conducted on three different tooth pairs for each wheel and pinion set.

The analysis of a test starts with the plotting of torque over time. To compare different gear sets, the torsional stiffness c_φ can be calculated within the range of linear-elastic material behavior by the quotient of the difference in torque ΔT and the difference of the angle $\Delta\varphi$ for the data of two timesteps according to equation (1):

$$c_\varphi = \frac{\Delta T}{\Delta \varphi} \tag{1}$$

2.4 Accompanying investigations

Along with the static loading tests, the manufactured gear quality and material properties were investigated with different

Figure 3 Static gear loading test rig

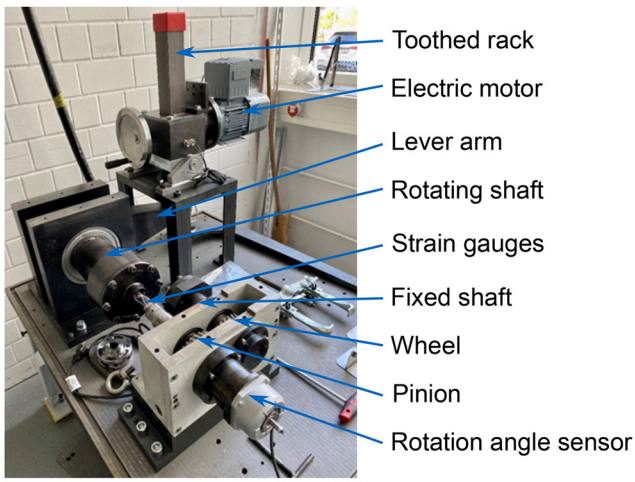

Source: By author

tools to identify the characteristics of additively manufactured gears. The macro- and microgeometry, as well as the surface roughness, were measured with tactile systems. Microsections were prepared to analyze the relative density, microstructure, case hardening depth (CHD) and hardness depth profile as well as the chemical composition. The relative density and microstructure were evaluated by an metallography expert with the help of an optical system. The visualization of the microstructure was conducted with a 2-percentage natal solution (98% ethanol, 2% nitric acid) as etching agent with an etching time of 20 s. The hardening depth and hardness depth profile were recorded with a microhardness test device. The chemical composition was identified by spark spectrometry.

3. Results

3.1 Static load testing

The testing procedure was conducted three times for each gear set. Figure 4 shows the increase and decrease of the torque over time for the variant LB-BO. An offset in time is applied to the results of tests 2 and 3 to obtain clear visibility of each curve. The curves for increasing and decreasing the load are asymmetric because loading is done at a slower speed than unloading. For each of the three tests, the maximum load of $T_1 = 1200$ Nm is achieved without observation of failure or plastic deformation. The slopes for loading and unloading the gears are comparable within the three tests showing a high reproducibility of the tests. For this gear geometry, the torque $T_1 = 1200$ Nm leads to a nominal contact stress $\sigma_{H0} \approx 2800$ N/mm^2 [according to ISO 6336-2 (2019)] and nominal tooth root stresses $\sigma_{F0,pinion} \approx 1950$ N/mm^2 and $\sigma_{F0,wheel} \approx 1850$ N/mm^2 [according to ISO 6336-3 (2019)], which are way above the load used for testing the pitting load-carrying capacity and tooth root bending strength.

Good reproducibility of the test results was also observed for the other variants. Each test reached the maximum torque $T_1 = 1200$ Nm without observing failure or plastic deformation. The gears' macro- and microgeometry measurements before and after the test confirmed the observed form stability.

Comparing the tests for the different variants reveals different torsional stiffnesses for each variant (Figure 5). Again, the curves are plotted with an offset in time for clear visibility of each curve. A steeper slope is equal to a higher torsional stiffness. Hence, the conventional and noLB variants are expected to have comparable torsional stiffness and higher torsional stiffness than the LB-T, LB-B, and LB-BO variants, which is confirmed by calculations.

The torsional stiffness was calculated according to equation (1) as an average during the loading phase in the linear-elastic material behavior of each 100 Nm between $T_1 = 200$ Nm and $T_1 = 1000$ Nm. The torsional stiffnesses with reference to the torque at the pinion are shown in Figure 6. It needs to be considered that the derived torsional stiffness refers to the whole system. The different tests differ in the lightweight structure of the gear wherefore the differences in torsional stiffness are theoretically only caused by the wheel variant. The conventionally manufactured gear set and noLB variant show nearly the same torsional stiffness. The gear sets with lightweight structures show less torsional stiffness in the following decreasing order: variant LB-B, variant LB-T, and variant LB-BO.

The torsional stiffnesses presented in Figure 6 are the mean value of three test runs with each eight evaluated torsional

Figure 4 Loading and unloading of the variant LB-BO gear set (curves of tests 2 and 3 with offset in time)

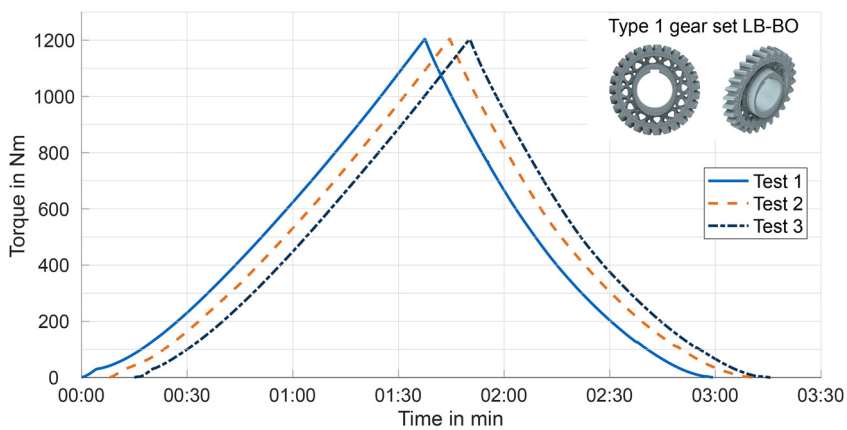

Source: By author

Figure 5 Loading and unloading of all variants in comparison (curves plotted with offset in time)

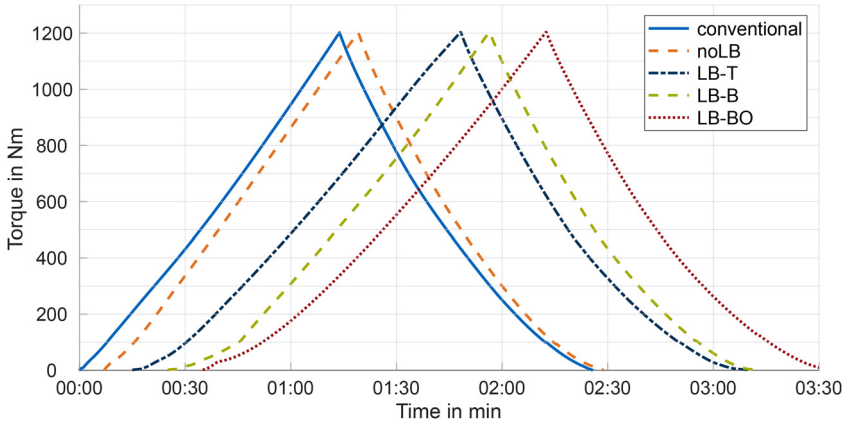

Source: By author

Figure 6 Comparison of the calculated torsional stiffness from the test data for the different variants

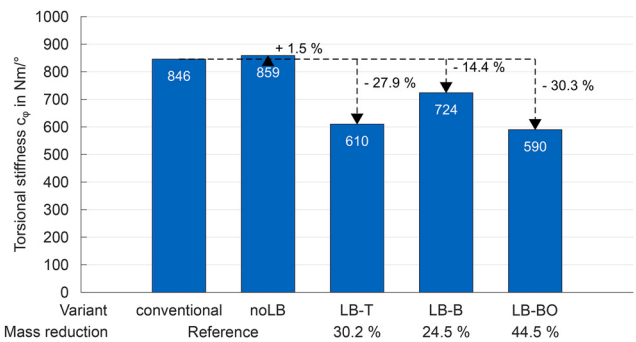

Source: By author

stiffnesses. The standard deviation for the lightweight variants (LB-T, LB-B, LB-BO) is within a range of ± 12 to 14%. For the conventionally manufactured variant, the standard deviation is ± 20%. A comparably high standard deviation of ± 36% is present for the variant noLB. A clear reason for the high standard deviations could not be identified. It is assumed that the angle measurement system is more prone to fluctuations for small changes in the angle at high torsional stiffnesses.

3.2 Gear quality and material properties

Different aspects regarding the gear quality and material properties were analyzed for the additively manufactured gears. The conventionally manufactured gear stem from another heat treatment batch than the additively manufactured gears. As the focus was to evaluate the characteristics of the additively manufactured gears, the characteristics of the conventionally manufactured gear are not presented in the following. Furthermore, quantitatively differences between additively and conventionally manufactured gears were not focus of this research. The qualitatively comparison of characteristics of additively manufactured gears and conventionally manufactured gears is based on the experience of the research institution.

3.2.1 Gear quality

Measurements classified the quality of the additively manufactured gears for characteristics like total profile deviation F_α, total helix deviation F_β, cumulative pitch deviation F_p, and runout F_r in quality 4 to 7 according to ISO 1328–1 (2013). The arithmetical mean roughness Ra was exemplary measured on three flanks of one gear and determined to be 0.34 μm. The achieved tooth flank roughness shows that PBF-LB/M manufactured gears are grindable like conventionally manufactured gears, resulting in suitable microgeometry and surface roughness. The quality of the gears produced by PBF-LB/M and processed according to Section 2.2 is comparable with conventionally manufactured gears.

The macrogeometry of the additively manufactured gears did not fully meet the specification due to shrinkage during the PBF-LB/M process. This was identified by measurements of the tip diameter and span, summarized in Table 3. The application of an adequate allowance can compensate for the shrinkage.

3.2.2 Relative density

The density was determined on polished microsections of selected samples. On average, the relative density is $\rho_{rel} > 99.7\%$. Hence, the gears have a relative density considerably above the target value of 99% according to VDI 3405-2 (2013) for

Table 3 Measurement results of the tip diameter and the span measurement of additively manufactured gears

Description	Symbol	Unit	Value	
			Pinion	Wheel
Tip diameter				
Specified value	d_a	mm	94.00 ± 0.1	101.00 ± 0.1
Measured value			93.758 ± 0.102	100.605 ± 0.046
Absolute difference			−0.242	−0.395
Span over 4 teeth				
Specified value	W_k	mm	$36.206^{-0.080}_{-0.118}$	$35.673^{-0.080}_{-0.118}$
Measured value			35.796 ± 0.027	35.180 ± 0.107
Absolute difference			−0.410	−0.493

Source: By author

additively manufactured parts. Two exemplary microsections with slightly different densities are shown in Figure 7.

3.2.3 Chemical composition

During the PBF-LB/M process, the energy input into the powder by the laser leads to the evaporation of chemical elements when the evaporation temperature is exceeded (Mukherjee *et al.*, 2016; Oliveira *et al.*, 2020). Elements like carbon can oxidize with residual oxygen to molecules such as CO and CO_2 (Rombouts *et al.*, 2006; Yang and Sisson, 2020). Due to these element volatilizations, the chemical composition of the used powder and the final part can differ. This is also observed with the variants investigated here. The chemical composition of the powder and the manufactured gears differ considerably (Table 4). The elements carbon, manganese, and silicon are lower by a fifth or even more, whereas the chromium content is higher than in the chemical composition of the powder. Compared with the chemical composition of 16MnCr5, specified in DIN EN ISO 683-3 (2019), the gears show a carbon content of 23% and a manganese content of 15% below the lower limit. Noteworthy is the aluminum content of 0.031 Wt.% in the additively manufactured gears in comparison with the amounts of phosphorus, sulfur and copper and their specified limits according to DIN EN ISO 683-3 (2019). The aluminum could result from impurities in the powder manufacturing, the handling of the powder or the PBF-LB/M process. It cannot be clearly determined where the contamination with aluminum happened as the aluminum content had not been determined for the powder. With the help of a scanning electron microscope, aluminum oxides were identified at the edge of pores. Further investigation is necessary to identify the correlation between the aluminum content and the porosity.

3.2.4 Case hardening depth and hardness depth profile

The CHD and the hardness depth profile were measured on microsections. The microsections were prepared parallel to the transverse section of the gear, and hardness measurements were conducted in the transverse section. The hardness measurement positions are comparable for all variants. Figure 8 visualizes exemplary the measurement positions on variant LB-BO. To determine the hardness depth profile perpendicular to the tooth flank (i.e. normal section), the obtained values were converted with the helix angle β according to equation (2):

Figure 7 Polished microsections with different relative densities taken from variant LB-B (left side) and variant LB-T (right side)

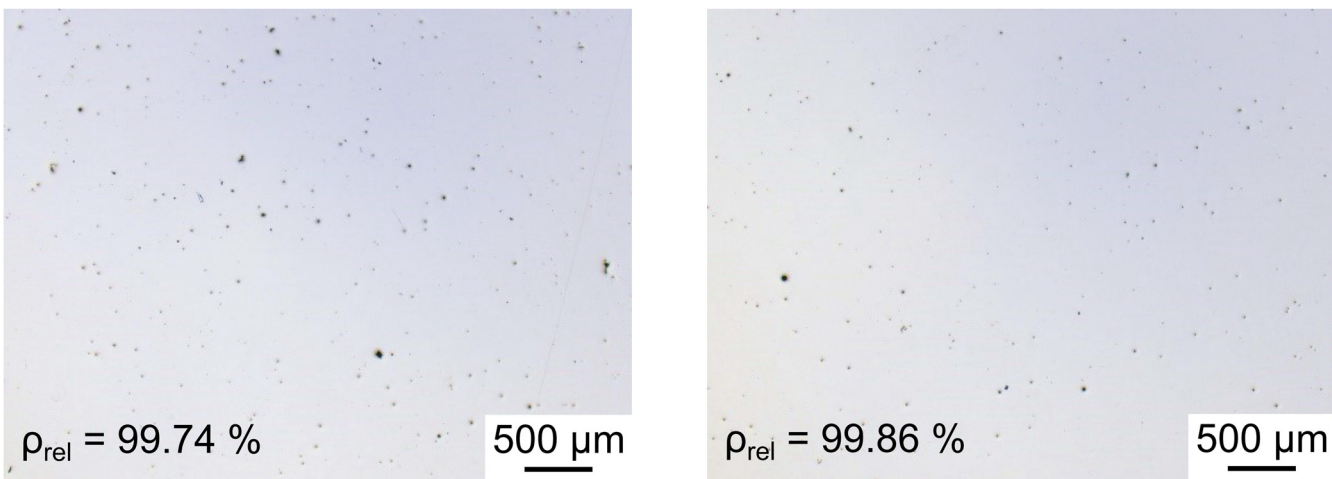

Source: By author

Table 4 Alloying elements for 16MnCr5 specified according to DIN EN ISO 683-3 (2019), measured by melt analysis for the powder and measured by spark spectrometry for the additively manufactured gears

Element	Element content specified for 16MnCr5 according to DIN EN ISO 683-3 (2019)	Element content measured in powder 16MnCr5 in Wt.%	Element content measured in gears in Wt.%	Deviation of gear compared to powder in %
Carbon C	0.14 – 0.19	0.15	0.108 ± 0.002	−28
Manganese Mn	1.00 – 1.30	1.05	0.852 ± 0.005	−19
Chromium Cr	0.80 – 1.10	0.9	0.960 ± 0.003	+7
Silicon Si	0.15 – 0.40	0.19	0.152 ± 0.002	−20
Phosphorus P	Max. 0.025	Not measured	0.014 ± 0.0003	
Sulfur S	Max. 0.035	Not measured	0.007 ± 0.0003	
Copper Cu	Max. 0.40	Not measured	0.016 ± 0.001	
Aluminum Al	Not specified	Not measured	0.031 ± 0.002	

Source: By author

Figure 8 Hardness measurement positions exemplary visualized on variant LB-BO

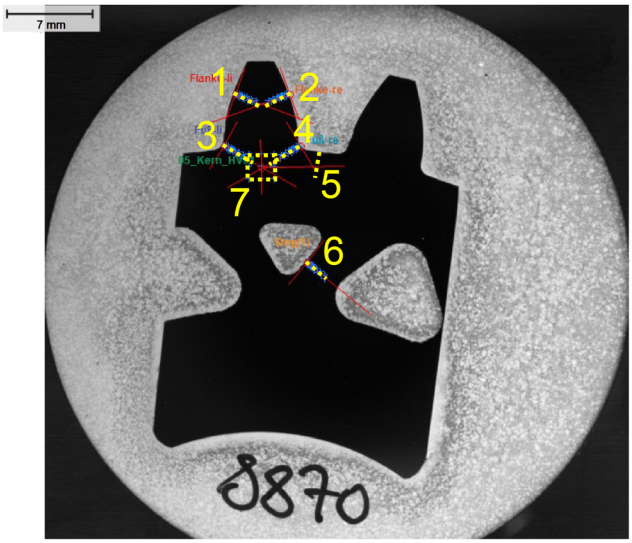

Notes: 1 Tooth flank left side, 2 Tooth flank right side, 3 Tooth root left side, 4 Tooth root right side, 5 Tooth root bottom, 6 Lightweight structure, 7 Core tooth center
Source: By author

$$t_n = t_t \cdot \cos\beta \tag{2}$$

Figure 9 shows the hardness depth profiles for all the gear variants at different measuring positions (left and right, tooth flank and tooth root, lightweight structure). For all variants, the hardness depth profile of the tooth root has a lower hardness compared to the tooth flanks at the same depth. The hardness depth profile of the lightweight structures is comparable with the hardness profile of the tooth flanks. The hardness depth profile for LB-T shows a significant rise of the measured hardness with the last measurement points. The lightweight structure of variant LB-T is thinner than the lightweight structure of variants LB-B and LB-BO. This leads to a higher hardness at the same depth and a rise in the hardness with the last two measuring points. This results from the fact, that the measuring depth surpasses the middle of the lightweight structure and the hardness rises again when getting closer to the other side.

Figure 10 details the measured hardness near the surface and the CHD at a hardness limit of 550 HV1 (CHD_{550HV}). The measurements on the left and right side of a tooth for the variants noLB and LB-T show comparable results. The slight differences in the CHD on the left and right side of the tooth for the variants LB-B and LB-BO presumably result from an asymmetric grinding process. The asymmetric grinding process was due to variations in the shrinkage of the additively manufactured gears and thus manual adjustments were needed to fully grind all flanks. A clear correlation between the lightweight structure and this behavior could not be identified. In general, the CHD in the tooth root is less than on the tooth flank. This observation is comparable to conventionally manufactured gears since the carbon diffusion into the tooth flank is less obstructed than in the tooth root. The microsections

Figure 9 Hardness depth profiles of the additively manufactured gears

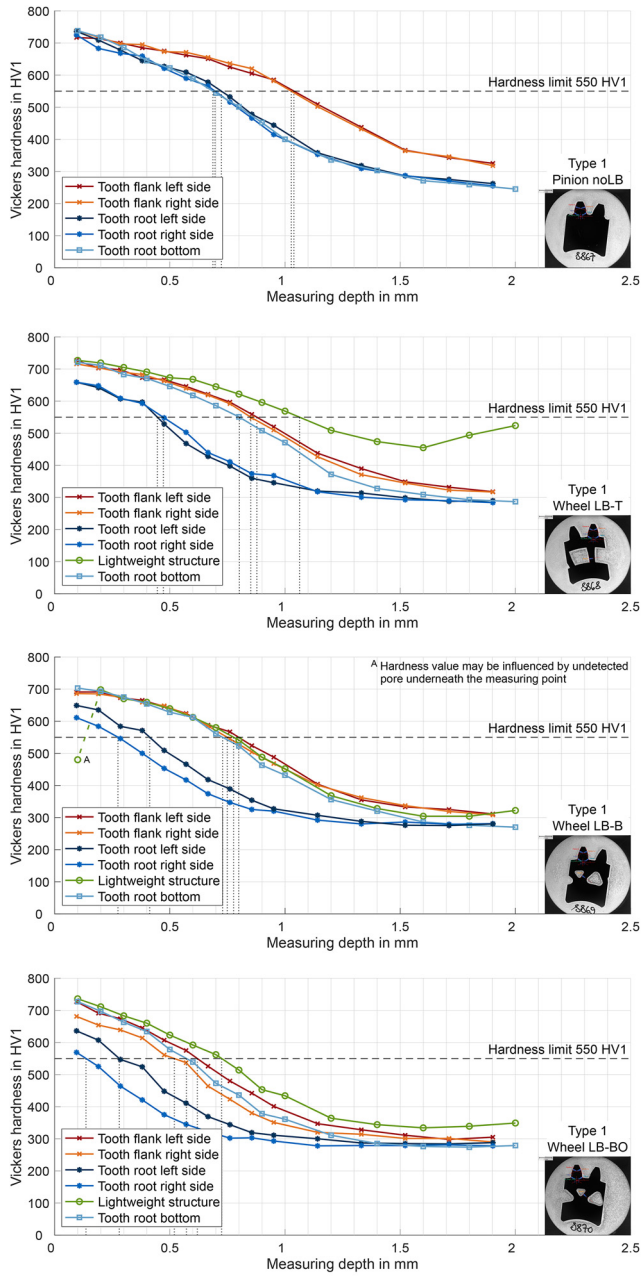

Source: By author

show high material removal by grinding in the tooth root (Figure 13).

The comparison of the case hardening depth of the additively manufactured gear variants reveals differences. The detailed analysis of the span corresponds with the observed differences in the case hardening depth. The variant noLB has the greatest and the variant LB-BO the least span, which means that more material, i.e. case hardened layer, was ground off. The additively manufactured gears showed a variable shrinkage during the PBF-LB/M process, thus leading to variable tooth flank grinding to fully grind the flanks and resulting in variable spans. The variable shrinkage may be an effect of the different

Figure 10 Measured hardness near the surface and case hardening depth at different positions

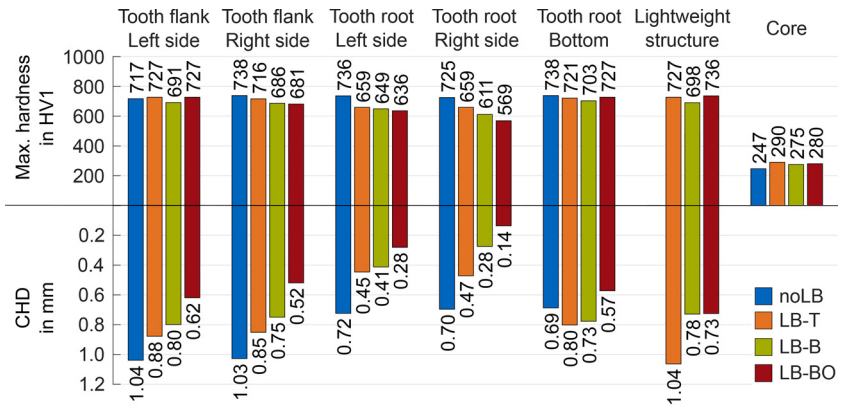

Source: By author

lightweight structures in the designs. With reduced mass, the cooling behavior in the additive manufacturing process is influenced that may cause a variation in shrinkage between the lightweight designs. Further studies are required to determine the dependency of shrinkage and lightweight design. In a serial production scenario, the shrinkage can be counteracted by scaling the gears or adjusting the beam-offset.

In summary, the hardness depth profile, maximum surface hardness, and CHD show some of the usual deviations resulting from the grinding process, but the quality of these characteristics is good and comparable.

3.2.5 Microstructure

The microstructure shows fine grains in the case-hardened layer and the core (Figure 11; Figure 12). The case-hardened layer is uniformly developed on all features of the gear, and the lightweight structure is not completely hardened through (Figure 13).

The case-hardened layer mainly consists of martensite with a fine and coarse needle structure and low proportions of bainite and retained austenite (Figure 11). These microstructural constituents are homogeneously distributed. The core shows

Figure 11 Microstructure in the tooth root area (left side) in variant LB-T

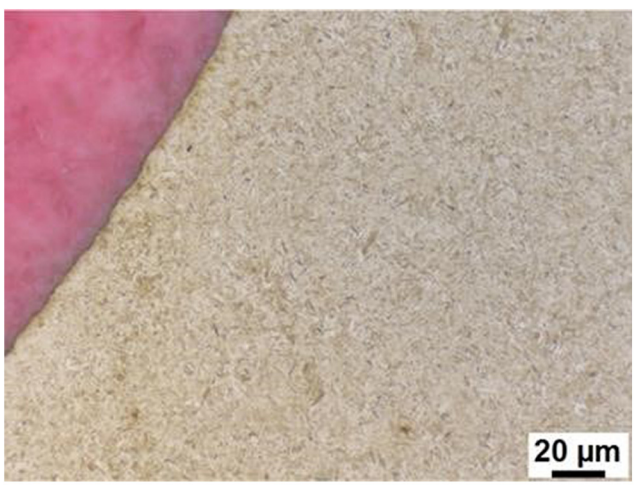

Source: By author

Figure 12 Microstructure in the core area of variant LB-B

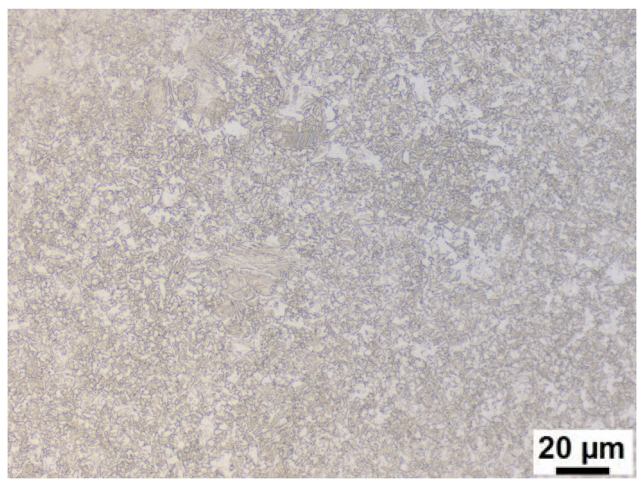

Source: By author

areas of upper bainite in a matrix of lower bainite (Figure 12). The upper bainite is to be found within the brighter areas with a slight brownish color. The white looking areas are also upper bainite, which cannot be fully seen due to the etching time and the resolution. The non-martensitic edge layer in non-ground surface areas mainly consists of troostite, retained austenite, and ferrite (Figure 16). Within all additively manufactured gears, the microstructure is comparable.

In general, the microstructure of the additively manufactured gears is comparable to the microstructure of conventionally manufactured gears. However, besides the similarity between additively and conventionally manufactured gears, some particularities were observed for the additively manufactured gears:

- In the case-hardened layer, there are sporadic, locally limited areas with coarse martensite needles surrounded by fine martensite needles (Figure 14). It is assumed that these inhomogeneities are induced by the PBF-LB/M process. Further investigation is ongoing for a comprehensive and sophisticated analysis of the origin.

Figure 13 Overview of the case hardening layer (brighter-appearing contour at surfaces) and microstructure on the features of the additively manufactured gear variants (each overview is put together by a series of square pictures which can be identified in this figure)

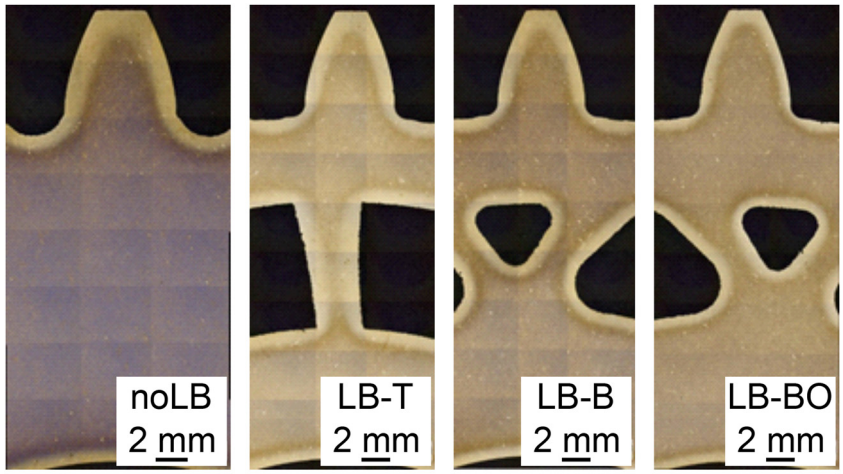

Source: By author

Figure 14 Inhomogeneities of the microstructure with coarse martensite needles at a tooth flank (right side) of variant LB-T

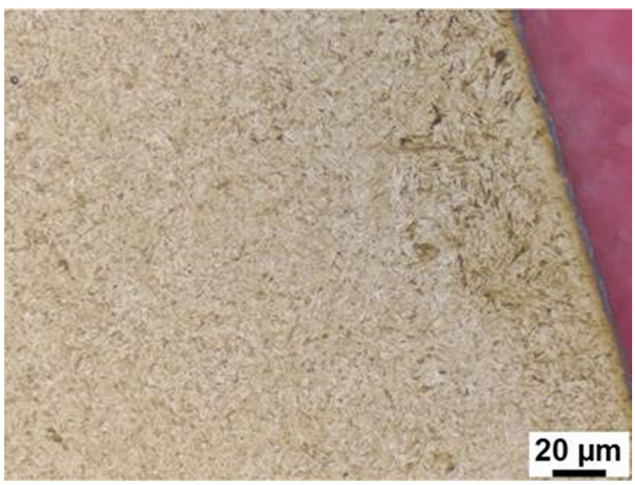

Source: By author

Figure 15 Bright spots showing aggregations of lower bainite or finer martensite than the surrounding material and also aggregations of aluminum oxide, manganese oxide or chromium at a tooth root (left side) of variant noLB (additionally observable: transition from the ground to the non-ground surface)

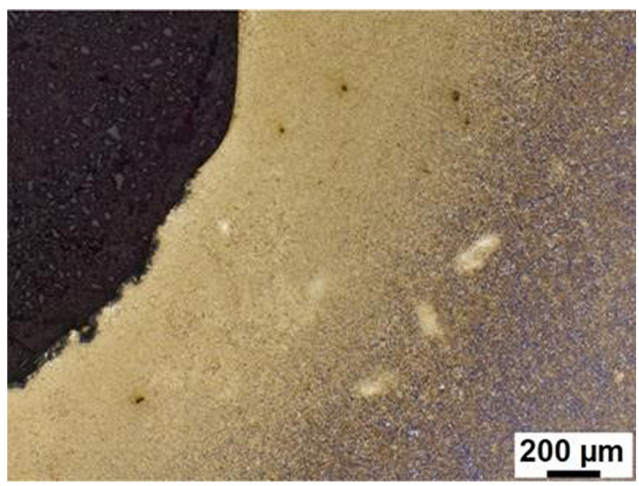

Source: By author

- Some spots in the microstructure of the additively manufactured gears occur brighter (Figure 15). Two different types were identified based on the possible resolution of the measuring system. The differences between these two types cannot be adequately picturized in this paper. Most of the bright spots consist of lower bainite or finer martensite than the surrounding material. Some bright spots did not respond properly to the etching liquid. With the help of a scanning electron microscope, these spots were identified as aluminum oxides, manganese oxides or chromium aggregations. The aggregations of external materials like aluminum could be caused by impurities in the powder (aluminum content was not determined for the powder; see Table 4) or by the multi-use of the PBF-LB/M machine and auxiliary equipment for different research projects with different materials. Despite thorough cleaning between two projects with different materials, minor residual amounts of external elements are inevitable. Remaining powder particles from previous building jobs with high-alloy steel could be the reason for the aggregations of manganese oxides and chromium.
- Non-ground surfaces have a highly uneven and coarse structure, and porosity near the surface is possible (Figure 16). The high surface roughness of the non-ground surfaces is caused by the PBF-LB/M process. During the static load testing, the high surface roughness in the tooth root did not adversely affect the load-carrying capacity.

Figure 16 High roughness of non-ground surface with near-surface pore and non-martensitic layer at the bottom of a tooth root of variant LB-BO

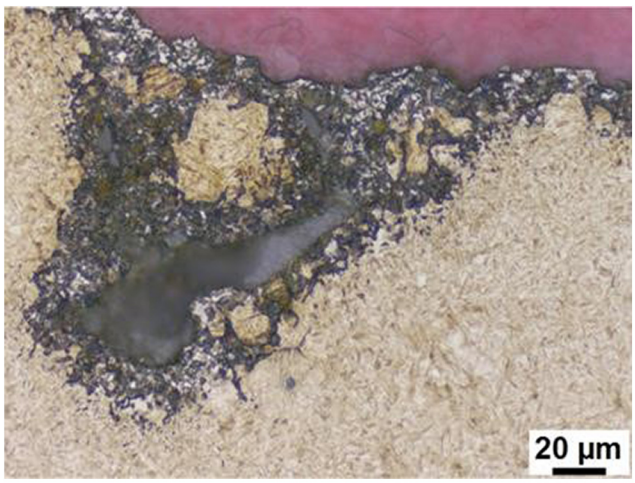

Source: By author

4. Discussion

4.1 Static load-carrying behavior of additively manufactured gears

The gears with different lightweight structures and mass savings of up to 45% showed no type of failure or plastic deformation up to an applied static torque of $T_1 = 1200$ Nm ($\sigma_{H0} \approx 2800\,N/mm^2$, $\sigma_{F0,pinion} \approx 1950\,N/mm^2$ $\sigma_{F0,wheel} \approx 1850\,N/mm^2$ according to ISO 6336-2 (2019) and ISO 6336-3 (2019)). The limiting factor of the static loading tests was the construction and dimensioning of the test rig. Previous attempts by Leonhardt *et al.* (2020) to reduce mass with variations of milled, forged, or formed gear hubs in combination with conventionally manufactured gear rims with similar dimensions [1] failed at torques $T_1 < 800$ Nm ($\sigma_{H0} \approx 2000\,N/mm^2$, $\sigma_{F0,pinion/wheel} \approx 1900\,N/mm^2$ according to ISO 6336-2 (2019) and ISO 6336-3 (2019)). The study of Leonhardt *et al.* (2020) showed that the greater the mass savings, the less static load could be handled. The additively manufactured gears tested cannot be ranked with the proposed trend as they are form stable regardless of the mass reduction up to the maximum testing torque. It could be possible, that for higher torques, the additively manufactured gears will show a decrease regarding the maximum static loading. The results of Leonhardt *et al.* (2020), as well as the results of this study, are shown in Figure 17. As all additively manufactured wheels with lightweight structures withstood a static torque of $T_1 = 1200$ Nm, there is proven potential for even more mass savings.

The evaluation of the torsional stiffness led to comparable values for the conventionally manufactured and the additively manufactured gear set without lightweight structures. Implementing lightweight structures led to a decrease of at least 14% in the torsional stiffness. However, a direct conclusion on the relationship between the amount of mass reduction and torsional stiffness cannot be drawn as different lightweight structures with the same degree of mass reduction can lead to different stiffnesses [see Mura *et al.* (2018): 2% mass difference achieved by two different lightweight structures, 180% increase in first natural frequency (directly related to stiffness)].

4.2 Gear quality and material properties of additively manufactured gears

The gear quality of the additively manufactured gears is comparable to conventionally manufactured gears. The same applies to the measured surface roughness on ground surfaces. The measurements of the macro- and microgeometry lead to the conclusion that the gear geometry differs from the specification (e.g., tip diameter, span). Despite the deviations, the gear geometry of the additively manufactured gears is still a proper gear geometry. The geometry can still be calculated by feeding gear designing and calculation software with the measured gear geometry data.

The additively manufactured gears show comparable but also some different material properties when compared with conventionally manufactured gears. On average, the investigated additively manufactured gears here show a relative density $\rho_{rel} > 99.7\%$. A significant difference in the relative density of the different gear variants was not observed.

The core hardness and microstructure differ slightly because of the change in the chemical composition during the PBF-LB/M process. The roughly 20% loss of both carbon and manganese leads to a core hardness of 273 HV1. In addition, the microstructure in the core shows less bainite because of the lower carbon content than in conventionally manufactured gears.

The surface hardness and the hardness depth profile are comparable with conventionally manufactured gears. Hence, the diffusivity of carbon into additively manufactured 16MnCr5 guarantees the development of an adequate

Figure 17 Static load-carrying capacity of additively manufactured gears in comparison with the results of Leonhardt *et al.* (2020)

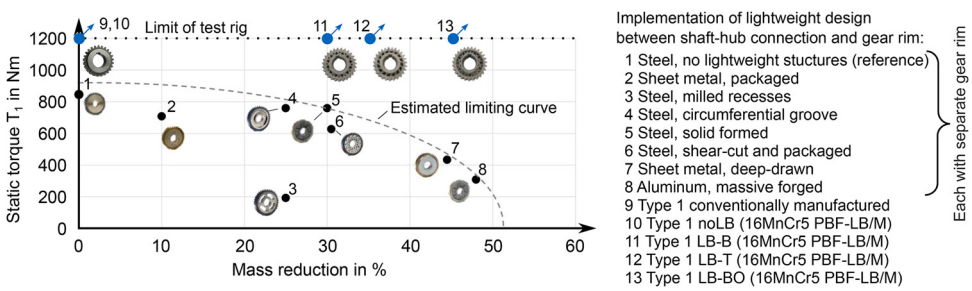

Source: By author

case-hardened layer. This was also observed for the case hardening steels 16MnCr5 and 20MnCr5 in other research (Bartels *et al.*, 2020; Schmitt *et al.*, 2020a; Schmitt *et al.*, 2020b; Yang and Sisson, 2020).

Further observations consider the occurrence of aggregations of aluminum oxide, manganese oxide, and chromium. The aluminum impurities might have been present in the powder, where the aluminum content was not determined (Table 4). Another theory is that the aluminum impurities might stem from former building jobs on the same PBF-LB/M machine or powder handling equipment. The latter is the likely reason for the aggregations of manganese oxide and chromium.

Despite the observed differences in the gear quality and material properties of additively manufactured gears compared to conventionally manufactured gears, no negative influence on the static load-carrying behavior could be identified in this research. The limit of the test rig was reached before failures of the additively manufactured gears could occur.

5. Summary, conclusion, and outlook

In this study, the static load-carrying behavior and material properties of additively manufactured gears with three different lightweight structures were investigated. The main results are the following:

- Despite a mass reduction of up to 45%, no failure or measurable plastic deformation in the additively manufactured gears was observed at a maximum static torque of $T_1 = 1200$ Nm. The limiting factor of the tests was the dimensioning of the static gear loading test rig.
- The additively manufactured gear sets with lightweight structures show a significantly lower torsional stiffness of at least −14% compared to gear sets without lightweight structures. Approximately the same torsional stiffness is achieved for a conventionally manufactured gear set and an additively manufactured gear set without lightweight structures.
- Shrinkage during the PBF-LB/M process leads to geometric deviations from the original gear dimensions. The tip diameter is roughly 0.3% smaller than specified. The shrinkage can be compensated for by the application of an adequate allowance.
- In general, the material properties of additively manufactured gears are comparable to conventionally manufactured gears, but some differences were also detected. Compared to conventionally manufactured gears, additively manufactured gears show lower relative density, lower core hardness, more inhomogeneities in the microstructure, and more impurities.
- The chemical composition between the powder and the produced gears differ. The main alloying elements, carbon and manganese, decrease by 28% and 19%. Compared with conventionally manufactured gears, the additively manufactured gears show a lower core hardness which can be related to the volatilization of alloying elements. However, the hardenability by case hardening of additively manufactured 16MnCr5 is still guaranteed.

In conclusion, this study proves a great static load-carrying capacity of additively manufactured gears. The evaluation of the maximum static load-carrying capacity was limited by the test rig. There is great potential in reducing the mass of gears with additively manufactured lightweight structures while maintaining a specified static load-carrying capacity. Future work should focus on characterizing and testing the dynamic load-carrying behavior of additively manufactured gears to allow the implementation of additively manufactured gears in future drivetrain applications. An increase in the power density is likely as the stability of additively manufactured gears with lightweight designs is given.

The accompanying investigations on the material and geometrical properties show the good state-of-the-art characteristics of additively manufactured gears. Equally, there is potential for improvement regarding the chemical composition, microstructure homogeneity, cleanliness, and compensation for shrinkage. Further research should be conducted on strategies for improving these characteristics.

Acknowledgments

The presented findings are based on the research project RE 1112/50–1 and STA 1198/10–1, funded by the *German Research Foundation* (Deutsche Forschungsgemeinschaft *e.V., DFG*). The authors would like to thank the *German Research Foundation* for its funding and support.

Gefördert durch
DFG Deutsche Forschungsgemeinschaft

This research project was substantially supported by the gear manufacturer *Wittmann GmbH – die Zahnradfabrik* and the heat treatment company *Wittmann Härterei GmbH*. The authors would like to thank *Wittmann GmbH – die Zahnradfabrik* and *Wittmann Härterei GmbH* for their generous support.

wittmann HÄRTEREI wittmann die Zahnradfabrik

Note

1 The macrogeometry in this research and the research of Leonhardt *et al.* (2020) is in several aspects comparable and the width of the lightweight structure is in the same range. No tooth root breakages were observed in the tests of Leonhardt *et al.* (2020). As the teeth are not the weak point of the gears, the full torque is transferred over the lightweight structure allowing a classification of the strength of the additively manufactured gears in comparison to the results of Leonhardt *et al.* (2020).

References

Bartels, D., Klaffki, J., Pitz, I., Merklein, C., Kostrewa, F. and Schmidt, M. (2020), "Investigation of the case-hardening behavior of additively manufactured 16MnCr5", *Metals*, Vol. 10 No. 4, pp. 536 1-12, doi: 10.3390/met10040536.

Brůžek, B. and Leidich, E. (2007), "'Dünnwandige verzahnte Naben mit Passfedernut' [Thin-Rimmed toothed hub with keyway]", *Welle-Nabe-Verbindungen. Gestaltung Fertigung*

Anwendungen [Shaft-Hub Connections. Design Manufacturing Application], Wiesloch Bei Heidelberg, VDI-Verlag (VDI Berichte, 2004), Düsseldorf, pp. 219–239, ISBN: 978-3-18-092004-7.

Bulduk, M.E., Çalışkan, C.İ., Coşkun, M., Özer, G. and Koç, E. (2022), "Comparison of the effect of different topological designs and process parameters on mechanical strength in gears", *The International Journal of Advanced Manufacturing Technology*, Vol. 119 Nos 9/10, pp. 6707-6716, doi: 10.1007/s00170-021-08405-4.

Concli, F. and Della Torre, A. (2021), "Impact of the LACKS of fusion induced by additive manufacturing on the lubrication of a gear flank", *Lubricants*, Vol. 9 No. 8, p. 83, doi: 10.3390/lubricants9080083.

DIN EN ISO 683-3 (2019), *Für eine Wärmebehandlung bestimmte Stähle, legierte Stähle und Automatenstähle – Teil 3: Einsatzstähle (ISO 683-3:2019); Deutsche Fassung EN ISO 683-3:2019 [Heat-treatable steels, alloy steels and free-cutting steels – Part 3: Case-hardening steels (ISO 683-3:2019); German version EN ISO 683-3:2019]* No. DIN EN ISO 683-3:2019-04.

Gebhardt, A. (2016), *Additive Fertigungsverfahren: Additive Manufacturing und 3D-Drucken für Prototyping – Tooling – Produktion [Additive Manufacturing Technologies – Additive Manufacturing and 3D-Printing for Prototyping – Tooling – Production]*, 5th ed., Carl Hanser Verlag, Munich, ISBN: 978-3-446-44401-0.

Gibson, I., Rosen, D., Stucker, B. and Khorasani, M. (2021), *Additive Manufacturing Technologies*, 3rd ed., Springer Nature, Switzerland, Cham, ISBN: 978-3-030-56126-0.

ISO 1328-1 (2013), Cylindrical gears – ISO system of flank tolerance classification – Part 1: Definitions and allowable values of deviations relevant to flanks of gear teeth No. ISO 1328-1:2013-09.

ISO 6336-2 (2019), Calculation of load capacity of spur and helical gears – Part 2: Calculation of surface durability (pitting) No. ISO 6336-2:2019-11.

ISO 6336-3 (2019), Calculation of load capacity of spur and helical gears – Part 3: Calculation of tooth bending strength No. ISO 6336-3:2019-11.

Kamps, T., Gralow, M., Schlick, G. and Reinhart, G. (2017), "Systematic biomimetic part design for additive manufacturing", *3rd CIRP Conference on BioManufacturing, Chicago, IL, Procedia CIRP*, Vol. 65, pp. 259-266, doi: 10.1016/j.procir.2017.04.054.

Kamps, T., Biedermann, M., Seidel, C. and Reinhart, G. (2018), "Design approach for additive manufacturing employing constructal theory for point-to-circle flows", *Additive Manufacturing*, Vol. 20, pp. 111-118, doi: 10.1016/j.addma.2017.12.005.

Kulangara, A.J., Rao, C.S.P. and Subhash Chandra Bose, P. (2018), "Generation and optimization of lattice structure on a spur gear", *7th International Conference of Materials Processing and Characterization (ICMPC 2017), Hyderabad, India, Materials Today: Proceedings*, Vol. 5 No. 2.1, pp. 5068-5073, doi: 10.1016/j.matpr.2017.12.085.

Leonhardt, C., Benkert, T., Meißner, R. and Otto, M. (2020), *FVA-Nr. 754/I – Massiver Leichtbau – Intelligenter Leichtbau durch Mehrkomponentenverfahren [LIGHTWEIGHTforging – Intelligent Lightweight Construction through Multi-Component Processes]*, Forschungsvereinigung Antriebstechnik e.V., Frankfurt am Main.

Milewski, J.O. (2017), *Additive Manufacturing of Metals: From Fundamental Technology to Rocket Nozzles, Medical Implants, and Custom Jewelry*, (Springer Series in Materials Science 258), 1st ed., Springer International Publishing, Cham, ISBN: 978-3-319-58205-4.

Mukherjee, T., Zuback, J.S., De, A. and DebRoy, T. (2016), "Printability of alloys for additive manufacturing", *Scientific Reports*, Vol. 6 No. 1, p. 19717, doi: 10.1038/srep19717.

Muminovic, A.J., Colic, M., Mesic, E. and Saric, I. (2020), "Innovative design of spur gear tooth with infill structure", *Bulletin of the Polish Academy of Sciences, Technical Sciences*, Vol. 68 No. 3, pp. 477-483, doi: 10.24425/bpasts.2020.133370.

Muminovic, A.J., Muminovic, A., Mesic, E., Saric, I. and Pervan, N. (2019), "Spur gear tooth topology optimization: finding optimal shell thickness for spur gear tooth produced using additive manufacturing", *TEM Journal*, Vol. 8 No. 3, pp. 788-794, doi: 10.18421/TEM83-13.

Mura, A., Curà, F. and Pasculli, L. (2018), "Optimisation methodology for lightweight gears to be produced by additive manufacturing techniques", *Proceedings of the Institution of Mechanical Engineers, Part C: Journal of Mechanical Engineering Science*, Vol. 232 No. 19, pp. 3512-3523, doi: 10.1177/0954406217737107.

Nguyen, D.S. and Vignat, F. (2016), "A method to generate lattice structure for additive manufacturing", *2016 IEEE International Conference on Industrial Engineering and Engineering Management (IEEM), Bali, Indonesia, IEEE*, pp. 966-970, doi: 10.1109/IEEM.2016.7798021.

Niemann, G. and Winter, H. (2003), *Maschinenelemente: Band 2: Getriebe allgemein, Zahnradgetriebe – Grundlagen, Stirnradgetriebe [Machine Elements – Volume 2: General Transmissions, Gearboxes – Fundamentals, Spur Gear Gearboxes]*, 2nd ed., Springer-Verlag, Berlin Heidelberg New York, NY, ISBN: 978-3-662-11874-0.

Oliveira, J.P., LaLonde, A.D. and Ma, J. (2020), "Processing parameters in laser powder bed fusion metal additive manufacturing", *Materials & Design*, Vol. 193, p. 108762, doi: 10.1016/j.matdes.2020.108762.

Ramandani, R., Belsak, A., Kegl, M., Predan, J. and Pehan, S. (2018), "Topology optimization based design of lightweight and low vibration gear bodies", *International Journal of Simulation Modelling*, Vol. 17 No. 1, pp. 92-104, doi: 10.2507/IJSIMM17(1)419.

Rombouts, M., Kruth, J.P., Froyen, L. and Mercelis, P. (2006), "Fundamentals of selective laser melting of alloyed steel powders", *CIRP Annals*, Vol. 55 No. 1, pp. 187-192, doi: 10.1016/S0007-8506(07)60395-3.

Schmitt, M., Kamps, T., Siglmüller, F., Winkler, J., Schlick, G., Seidel, C., Tobie, T., Stahl, K. and Reinhart, G. (2020a), "Laser-based powder bed fusion of 16MnCr5 and resulting material properties", *Additive Manufacturing*, Vol. 35, p. 101372, doi: 10.1016/j.addma.2020.101372.

Schmitt, M., Jansen, D., Bihlmeir, A., Winkler, J., Anstätt, C., Schlick, G., Tobie, T., Stahl, K. and Reinhart, G. (2019), "Rahmen und Strategien für den Leichtbau von additiv

gefertigten Zahnrädern für die Automobilindustrie [Framework and strategies for the lightweight construction of AM gears for the automotive industry]", in Kynast, M., Eichmann, M. and Witt, G. (Eds), *Rapid.Tech + FabCon 3. D – International Hub for Additive Manufacturing: Exhibition + Conference + Networking (Proceedings of the 16th Rapid. Tech Conference Erfurt, Germany)*, *Erfurt, Germany, Carl Hanser Verlag, Munich*, pp. 89-102, doi: 10.3139/9783446462441.007.

Schmitt, M., Kempter, B., Inayathulla, S., Gottwalt, A., Horn, M., Binder, M., Winkler, H., Schlick, G., Tobie, T., Stahl, K. and Reinhart, G. (2020b), "Influence of baseplate heating and shielding gas on distortion, mechanical and case hardening properties of 16MnCr5 fabricated by laser powder bed fusion", *53rd CIRP Conference on Manufacturing Systems 2020, Virtual Conference (Chicago, IL)*, Procedia CIRP, Vol. 93, pp. 581-586, doi: 10.1016/j.procir.2020.03.089.

VDI 3405-2 (2013), Additive Fertigungsverfahren – Strahlschmelzen metallischer Bauteile – Qualifizierung, Qualitätssicherung und Nachbearbeitung [Additive manufacturing processes, rapid manufacturing – Beam melting of metallic parts – Qualification, quality assurance and post processing] No. VDI 3405-2:2013-08.

Winkler, K.J., Schmitt, M., Tobie, T., Schlick, G., Stahl, K. and Daub, R. (2023), "Characterization and Influences of the Load Carrying Capacity of Lightweight Hub Designs of 3D-Printed Gears (16MnCr5, PBF-LB/M-Process)", in Rieser, J., Endress, F., Horoschenkoff, A., Höfer, P., Dickhut, T. and Zimmermann, M. (Eds), *Proceedings of the Munich Symposium on Lightweight Design 2021*, *Munich, Germany*, *Springer Vieweg, Berlin, Heidelberg*, pp. 160-174, doi: 10.1007/978-3-662-65216-9_15.

Yang, M. and Sisson, R.D. Jr., (2020), "Carburizing Heat Treatment of Selective-Laser-Melted 20MnCr5 Steel", *Journal of Materials Engineering and Performance*, Vol. 29 No. 6, pp. 3476-3485, doi: 10.1007/s11665-020-04564-9.

Corresponding author

Markus Brummer can be contacted at: markus.brummer@tum.de

For instructions on how to order reprints of this article, please visit our website:
www.emeraldgrouppublishing.com/licensing/reprints.htm
Or contact us for further details: **permissions@emeraldinsight.com**